

Communication

Theoretical Investigation of Bandwidth in Multimode Step-Index Silica Photonic Crystal Fibers

Branko Drljača ¹ , Svetislav Savović ^{2,3}, Milan S. Kovačević ², Ana Simović ², Ljubica Kuzmanović ²,
Alexandar Djordjevich ³ and Rui Min ^{4,*} 

¹ Faculty of Sciences and Mathematics, University of Priština in Kosovska Mitrovica, L. Ribara 29, 38220 Kosovska Mitrovica, Serbia; branko.drljaca@pr.ac.rs

² Faculty of Science, University of Kragujevac, R. Domanovića 12, 34000 Kragujevac, Serbia; savovic@kg.ac.rs (S.S.); kovac@kg.ac.rs (M.S.K.); asimovic@kg.ac.rs (A.S.); ljubica.kuzmanovic@pmf.kg.ac.rs (L.K.)

³ Department of Mechanical Engineering, City University of Hong Kong, Hong Kong, China; mealex@cityu.edu.hk

⁴ Center for Cognition and Neuroergonomics, State Key Laboratory of Cognitive Neuroscience and Learning, Beijing Normal University at Zhuhai, Zhuhai 519087, China

* Correspondence: ruimin@bnu.edu.cn

Abstract: Solving the time-dependent power flow equation (PFE) provides a useful method to study the transmission bandwidth of step-index silica photonic crystal fibers (SI SPCFs). The transmission bandwidth of these kinds of fibers is determined for different air-hole structures (different numerical apertures (NAs)) and different distribution widths of the Gaussian launch beam. The results indicate that the lower the NA of SI SPCFs, the higher the bandwidth (for example, for a lower NA of SI SPCFs, a bandwidth that is eight times larger is obtained at a fiber length of 3500 m). The narrower launch beam at short fiber lengths results in a wider bandwidth. The longer the fiber (>300 m), the much less the effect of the launch beam width on the bandwidth. The bandwidth becomes independent of the width of the launch beam distribution at the fiber length at which a steady-state distribution (SSD) is reached. These results are useful for some potential applications, such as high capacity transmission optical fiber systems.

Keywords: photonic crystal fiber; bandwidth; multimode optical fiber; step-index fiber; power flow equation



Citation: Drljača, B.; Savović, S.; Kovačević, M.S.; Simović, A.; Kuzmanović, L.; Djordjevich, A.; Min, R. Theoretical Investigation of Bandwidth in Multimode Step-Index Silica Photonic Crystal Fibers.

Photonics **2022**, *9*, 214. <https://doi.org/10.3390/photonics9040214>

Received: 28 February 2022

Accepted: 22 March 2022

Published: 23 March 2022

Publisher's Note: MDPI stays neutral with regard to jurisdictional claims in published maps and institutional affiliations.



Copyright: © 2022 by the authors. Licensee MDPI, Basel, Switzerland. This article is an open access article distributed under the terms and conditions of the Creative Commons Attribution (CC BY) license (<https://creativecommons.org/licenses/by/4.0/>).

1. Introduction

The communication system based on optical fibers provides more reliability and flexibility than the wireless communication medium, which is the backbone of the modern telecommunication network [1]. The PCF first investigated by the Russell group is a specific optical fiber technology (optical fiber with micro-structure) for light guiding [2]. The light passing through PCFs follows two principles: the first one is light passing through a high refractive index (RI) medium surrounded by a lower RI medium, and the other one is light passing through a low RI medium surrounded by a higher RI medium. For some kinds of PCFs, a high RI material, such as silica material, is implemented as the background material, which is doped in a periodic manner with air holes. The hole pattern has lowered the effective RI of the fiber cladding and allows the optical fibers to guide light [2–7]. Choosing this cladding hole pattern allows one to adjust the RI profile of the optical fiber during the design process. PCFs exhibit excellent performance as the microstructure of the fibers provides additional flexibility to influence the cross-section during the design phase. The “end-less” PCF [2] has been shown to work only in fundamental mode over a wide range of wavelengths. On the other hand, a PCF may have an empty core. Photonic gap guidance [8–11] allows the “air center” of hollow fibers to have a lower RI than the RI of

the cladding material [12,13]. In practice, optical dispersion and birefringence of PCFs is often investigated [14–17]. Nowadays, PCFs are important since they can be implemented for many applications, such as supercontinuum light generation [18–20], light wavelength conversion [21,22], optical fluids [23], and different sensing area [24]. The width of the PCF material between the holes of the cladding determines the NA of the PCF, which is normally limited to $NA \simeq 0.5\text{--}0.6$ [25–27]. Sometimes, PCFs considered include heavy metal oxide glass fibers [28] and liquid-filled hollow-core fibers for specific applications [29]. Additionally, high NA PCFs demonstrated excellent resolution in lensless focusing [30].

PCFs show high bandwidth performance and flexibility, making them useful for transmission and sensing technology. The propagation characteristics of PCFs are important parameters for their practical applications, which are affected by mode attenuation, mode coupling, and modal dispersion. The main cause of mode coupling lies in light scattering due to intrinsic perturbations in the fiber (micro-bend, changes in diameter, and changes in density and RI distribution). One of the most efficient approaches in modeling the transmission characteristics of multimode optical fibers is based on the employment of the PFE [31–36]. In this work, by solving the time-dependent PFE, we determine the bandwidth of a multimode SI SPCF with a solid core for two different launch beam distribution widths and two different air-hole sizes (two different NAs), which have a great potential for applications in optical fiber communication. The central part has the highest RI; holes with diameter d and pitch Λ in the cladding reduce the effective value of RI in the cladding.

2. The Design of the PCF

Here, we present a SI PCF design in which the air holes are uniform in size and form an equilateral triangular network in the cladding, as shown in Figure 1. Despite the fact that the material properties are uniform throughout the optical fiber, the hole-free central part has the highest RI; holes with diameter d and pitch Λ in the cladding reduce the effective value of RI in the cladding.

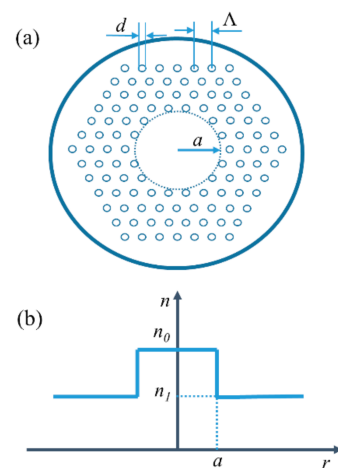


Figure 1. (a) Lateral end-face of a solid-core multimode SI PCF, where Λ is the pitch and d is the diameter of the air holes. (b) RI profile of a multimode SI PCF.

3. The Time-Dependent PFE

We used the time-dependent PFE for the bandwidth simulation, which is presented in the following form [31]:

$$\frac{\partial p(\theta, z, t)}{\partial z} + \tau(\theta) \frac{\partial p(\theta, z, t)}{\partial t} = -\alpha(\theta)P(\theta, z, t) + \frac{1}{\theta} \frac{\partial}{\partial \theta} \left[D(\theta) \frac{\partial p(\theta, z, t)}{\partial \theta} \right] \quad (1)$$

where t is the time, θ is the angle, z is the optical fiber length, $p(\theta, z, t)$ is the power distribution, $\tau(\theta)$ is the modal delay, $D(\theta)$ is the coupling coefficient (usually assumed constant [31,32]), and $\alpha(\theta) \simeq \alpha_0$ (it does not have to be accounted when solving (1)) [32].

The Fourier transformation of Equation (1) is:

$$\frac{\partial P(\theta, z, \omega)}{\partial z} + j\omega\tau(\theta)P(\theta, z, \omega) = -\alpha(\theta)P(\theta, z, \omega) + \frac{1}{\theta} \frac{\partial}{\partial \theta} \left[\theta D(\theta) \frac{\partial P(\theta, z, \omega)}{\partial \theta} \right] \quad (2)$$

where $\omega = 2\pi f$ is the angular frequency, and we obtain:

$$P(\theta, z, \omega) = \int_{-\infty}^{+\infty} p(\theta, z, t) \exp(-j\omega t) dt \quad (3)$$

The boundary conditions are presented in the following form:

$$P(\theta_m, z, \omega) = 0, D(\theta) \frac{\partial P(\theta, z, \omega)}{\partial \theta} \Big|_{\theta=0} = 0 \quad (4)$$

Since $P(\theta, z, \omega)$ has the real part $P_r(\theta, z, \omega)$ and imaginary part $P_i(\theta, z, \omega)$, Equation (2) can be rewritten as:

$$\begin{aligned} \frac{\partial P_r(\theta, z, \omega)}{\partial z} &= -\alpha(\theta)P_r(\theta, z, \omega) + \frac{D}{\theta} \frac{\partial P_r(\theta, z, \omega)}{\partial \theta} + D \frac{\partial^2 P_r(\theta, z, \omega)}{\partial \theta^2} + \omega\tau P_i(\theta, z, \omega) \\ \frac{\partial P_i(\theta, z, \omega)}{\partial z} &= -\alpha(\theta)P_i(\theta, z, \omega) + \frac{D}{\theta} \frac{\partial P_i(\theta, z, \omega)}{\partial \theta} + D \frac{\partial^2 P_i(\theta, z, \omega)}{\partial \theta^2} - \omega\tau P_r(\theta, z, \omega) \end{aligned} \quad (5)$$

where

$$P(\theta, z, \omega) = P_r(\theta, z, \omega) + jP_i(\theta, z, \omega) \quad (6)$$

We obtained $P_r(\theta, z, \omega)$ and $P_i(\theta, z, \omega)$ by numerically solving Equation (5) using the explicit finite difference method (EFDM). The frequency response $H(z, \omega)$ is then obtained as:

$$H(z, \omega) = \frac{2\pi \int_0^{\theta_m} \theta [P_r(\theta, z, \omega) + jP_i(\theta, z, \omega)] d\theta}{2\pi \int_0^{\theta_m} \theta [P_r(\theta, 0, \omega) + jP_i(\theta, 0, \omega)] d\theta} \quad (7)$$

This equation can be used to determine the change of the transmission bandwidth with the transmission length.

4. Simulation Results

The bandwidth for various launch beam distribution widths in the multimode SI SPCF was investigated. For a PCF with triangular lattice air holes, the effective parameter V is presented as:

$$V = \frac{2\pi}{\lambda} a_{eff} \sqrt{n_0^2 - n_{fsm}^2} \quad (8)$$

where n_0 is the RI of the core, n_{fsm} is the effective RI of the cladding, and $a_{eff} = \Lambda/\sqrt{3}$ [33]. The effective RI of the cladding $n_1 \equiv n_{fsm}$, can be obtained from Equation (8), using the following equation [33]:

$$V \left(\frac{\lambda}{\Lambda}, \frac{d}{\Lambda} \right) = A_1 + \frac{A_2}{1 + A_3 \exp(A_4 \lambda / \Lambda)} \quad (9)$$

where the parameters for fitting A_i ($i = 1$ to 4) are presented as:

$$A_i = a_{i0} + a_{i1} \left(\frac{d}{\Lambda} \right)^{b_{i1}} + a_{i2} \left(\frac{d}{\Lambda} \right)^{b_{i2}} + a_{i3} \left(\frac{d}{\Lambda} \right)^{b_{i3}} \quad (10)$$

where the coefficients a_{i0} to a_{i3} and b_{i1} to b_{i3} ($i = 1$ to 4) are supplied in Table 1.

Table 1. Fitting coefficients in Equation (10) [33].

	<i>i</i> =1	<i>i</i> =2	<i>i</i> =3	<i>i</i> =4
a_{i0}	0.54808	0.71041	0.16904	−1.52736
a_{i1}	5.00401	9.73491	1.85765	1.06745
a_{i2}	−10.43248	47.41496	18.96849	1.93229
a_{i3}	8.22992	−43.750962	−42.4318	3.89
b_{i1}	5	1.8	1.7	−0.84
b_{i2}	7	7.32	10	1.02
b_{i3}	9	22.8	14	13.4

Figure 2 shows the cladding’s effective RI $n_1 \equiv n_{fsm}$ as a function of λ/Λ , for $\Lambda = 3 \mu\text{m}$ and for two values of the hole diameter d . The design parameters of the investigated SI SPCF are presented in Table 2.

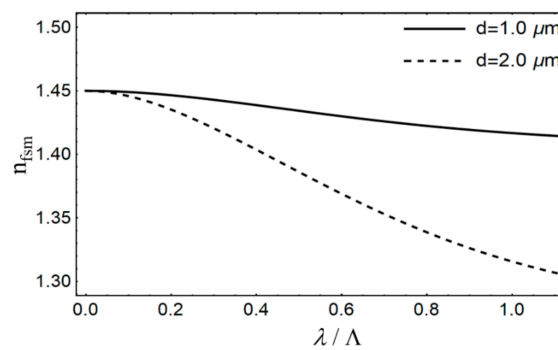


Figure 2. Effective RI of the inner cladding as a function of λ/Λ .

Table 2. Effective RI of the cladding n_1 , relative RI difference $\Delta = (n_0 - n_1)/n_0$, where $n_0 = 1.45$, and the critical angle θ_m for the varied air-hole diameter d at wavelength 850 nm.

<i>d</i> (μm)	1.0	2.0
n_1	1.443717	1.423679
$\Delta = (n_0 - n_1)/n_0$	0.00433	0.01815
θ_m (deg)	5.34	10.93

The Equation (5) are solved using the EFDM [34], where the coupling coefficient was $D = 2.3 \times 10^{-6} \text{rad}^2/\text{m}$ (typical value of D for glass core fibers [35]). The cases with diameter of air holes $d = 1 \mu\text{m}$ ($n_1 = 1.443717$, $\Delta = 0.00433$) and $d = 2 \mu\text{m}$ ($n_1 = 1.423679$, $\Delta = 0.01815$) and launch beam distribution with $(\text{FWHM})_{z=0} = 1^\circ$ and 5° are analyzed.

For illustration purposes, Figure 3 shows the bandwidth expansion over the fiber length. This was calculated for the beam distributions with $(\text{FWHM})_{z=0} = 1^\circ$ and 5° , in the case of $\Delta = 0.00433$ and $\Delta = 0.01815$. From Figure 3, we can observe that a lower NA (smaller Δ) yields a higher bandwidth. For shorter fiber lengths, the smaller the Gaussian launch beam width, the wider the bandwidth. This is due to the narrow launch beam of $(\text{FWHM})_{z=0} = 1^\circ$, which reduces the modal dispersion. The effect of the $(\text{FWHM})_{z=0}$ of the launch beam distribution on the bandwidth vanishes with increasing the optical fiber length. Initial mode excitation has less effect on the bandwidth of longer fibers, because mode coupling affects the redistribution of energy between guide modes. Figure 3 shows a linear decrease in the bandwidth over short fiber lengths before switching to a $1/z^{1/2}$ functional dependence. For the larger widths of the Gaussian launch beams and lower NAs, this change, and therefore the equilibrium mode distribution, occurs at shorter fiber lengths. For $(\text{FWHM})_{z=0} = 1^\circ$, the length is $L_c \simeq 500 \text{ m}$ for $n_1 = 1.443717$ and $L_c \simeq 1650 \text{ m}$ for $n_1 = 1.423679$. For $(\text{FWHM})_{z=0} = 5^\circ$, the length is $L_c \simeq 300 \text{ m}$ for $n_1 = 1.443717$ and $L_c \simeq 1450 \text{ m}$ for $n_1 = 1.423679$ [36]. The shorter the length L_c , the slower the bandwidth

decrease. The bandwidth tends to be length-independent for certain fiber lengths. This length marks the onset of an SSD. This length is $z_{SSD} \approx 1150$ m for $n_1 = 1.443717$ and $z_{SSD} \approx 3800$ m for $n_1 = 1.423679$ [36]. Finally, one can conclude that the examined PCFs seem to be suitable for short-haul rather than long-haul applications.

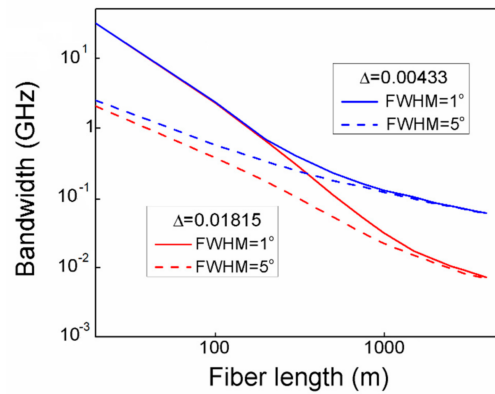


Figure 3. Bandwidth as a function of the optical fiber length for the Gaussian launch beams with $(FWHM)_{z=0} = 1^\circ$ and 5° for $\Delta = 0.00433$ $\Delta = 0.01815$.

It is worth noting that the proposed method for the investigation of the bandwidth in SI SPCFs by employing the time-dependent power flow equation has already been proven as effective and accurate in several previously published works, including the theoretical and experimental investigation of bandwidths in graded-index plastic optical fibers and SI plastic optical fibers [34,37]. A block diagram that illustrates the procedure applied in this work for the calculation of the bandwidth in SI SPCFs is shown in Figure 4.

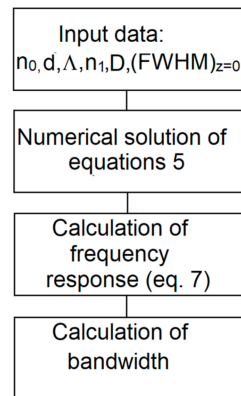


Figure 4. Block diagram for the calculation of the bandwidth in SI SPCFs.

5. Conclusions

To conclude, by solving the time-dependent PFE, an approach for estimating the bandwidth of multimode SI SPCFs is proposed. From the obtained results, we conclude that lower NA enables a higher fiber bandwidth (e.g., for lower NA of SI SPCFs, a bandwidth that is eight times larger is obtained at a fiber length of 3500 m). Additionally, a narrower Gaussian launch beam leads to a higher bandwidth at short fiber lengths. The bandwidth decreases with increasing the fiber length and tends to be launch-beam independent for a certain fiber length. This length marks the onset of the SSD. One can conclude that the examined PCFs seem to be suitable for short-haul rather than long-haul applications. Finally, we show that these tuning parameters provide additional flexibility in the construction of photonic crystal fibers for high bandwidth optical fiber transmission.

Author Contributions: Methodology, software, B.D. and M.S.K.; writing—original draft preparation, S.S., L.K. and A.S.; writing—review and editing, A.D., S.S. and R.M.; funding acquisition, S.S. and R.M. All authors have read and agreed to the published version of the manuscript.

Funding: This research was funded by the NSFC (62003046, 6211101138); City University of Hong Kong (CityU 7004600); Serbian Ministry of Education, Science and Technological Development (451-03-68/2022-14/200122); Science Fund of the Republic of Serbia (CTPCF-6379382); Guangdong Provincial Department of Technology (2021A1515011997); Guangdong Provincial Department of Education (2021ZDZX1050,2021KCXTD014); and Guangdong Provincial Department of Science and Technology(2021A1313030055).

Institutional Review Board Statement: Not applicable.

Informed Consent Statement: Not applicable.

Data Availability Statement: The data presented in this study are available on request from the corresponding author.

Conflicts of Interest: The authors declare no conflict of interest.

References

1. Knight, J.C.; Birks, T.A.; Russell, P.S.J.; Atkin, D.M. All-silica single-mode optical fiber with photonic crystal cladding. *Opt. Lett.* **1996**, *21*, 1547–1549. [[CrossRef](#)] [[PubMed](#)]
2. Birks, T.A.; Knight, J.C.; Russell, P.S.J. Endlessly single-mode photonic crystal fiber. *Opt. Lett.* **1997**, *22*, 961–963. [[CrossRef](#)] [[PubMed](#)]
3. Russell, P.S.J. Photonic crystal fibers. *Science* **2003**, *299*, 358–362. [[CrossRef](#)] [[PubMed](#)]
4. Knight, J.C. Photonic crystal fiber. *Nature* **2003**, *424*, 847–851. [[CrossRef](#)]
5. Russell, P.S.J. Photonic-crystal fibers. *J. Lightwave Technol.* **2006**, *24*, 4729–4749. [[CrossRef](#)]
6. Knight, J.C.; Broeng, J.; Birks, T.A.; Russell, P.S.J. Photonic Band Gap Guidance in Optical Fibers. *Science* **1998**, *282*, 1476–1478. [[CrossRef](#)]
7. Knight, J.C.; Russell, P.S.J. Photonic crystal fibers: New way to guide light. *Science* **2002**, *296*, 276–277. [[CrossRef](#)]
8. Cregan, R.F.; Mangan, B.J.; Knight, J.C.; Birks, T.A.; Russell, P.S.J.; Roberts, P.J.; Allan, D.C. Single-Mode Photonic Band Gap Guidance of Light in Air. *Science* **1999**, *285*, 1537–1539. [[CrossRef](#)]
9. Amezcua-Correa, R.; G er ome, F.; Leon-Saval, S.; Broderick, N.G.R.; Birks, T.; Knight, J. Control of surface modes in low loss hollow-core photonic bandgap fibers. *Opt. Express* **2008**, *16*, 1142–1149. [[CrossRef](#)]
10. Zhang, Z.; He, J.; Du, B.; Guo, K.; Wang, Y. Highly sensitive gas refractive index sensor based on hollow-core photonic bandgap fiber. *Opt. Express* **2009**, *27*, 29649–29658. [[CrossRef](#)]
11. Zhang, X.; Gao, S.; Wang, Y.; Ding, W.; Wang, X.; Wang, P. 7-cell hollow-core photonic bandgap fiber with broad spectral bandwidth and low loss. *Opt. Express* **2019**, *27*, 11608–11616. [[CrossRef](#)]
12. Benabid, F.; Knight, J.C.; Antonopoulos, G.; Russell, P.S.J. Stimulated Raman Scattering in Hydrogen-Filled Hollow-Core Photonic Crystal Fiber. *Science* **2002**, *298*, 399–402. [[CrossRef](#)]
13. Light, P.; Benabid, F.; Couny, F.; Maric, M.; Luiten, A. Electromagnetically induced transparency in Rb-filled coated hollow-core photonic crystal fiber. *Opt. Lett.* **2007**, *32*, 1323–1325. [[CrossRef](#)]
14. Mogilevtsev, D.; Birks, T.; Russell, P. Group-velocity dispersion in photonic crystal fibers. *Opt. Lett.* **1998**, *23*, 1662–1664. [[CrossRef](#)]
15. Nair, A.A.; Amiri, I.S.; Boopathi, C.S.; Karthikumar, S.; Jayaraju, M.; Yupapin, P. Numerical investigation of co-doped microstructured fiber with two zero-dispersion wavelengths. *Results Phys.* **2018**, *10*, 766–771. [[CrossRef](#)]
16. Huang, Y.; Yang, H.; Zhao, S.; Mao, Y.; Chen, S. Design of photonic crystal fibers with flat dispersion and three zero dispersion wavelengths for coherent supercontinuum generation in both normal and anomalous regions. *Results Phys.* **2021**, *23*, 104033. [[CrossRef](#)]
17. Anas, T.; Asaduzzaman, S.; Ahmed, K.; Bhuiyan, T. Investigation of highly birefringent and highly nonlinear Hexa Secteded PCF with low confinement loss. *Results Phys.* **2018**, *11*, 1039–1043. [[CrossRef](#)]
18. Rajesh, A.; Chandru, S.; Robinson, S. Investigation of defective hybrid cladding with silicon nanocrystal PCF for super-continuum generation. *Laser Phys.* **2021**, *31*, 126206. [[CrossRef](#)]
19. Kuliesaitė, M.; Jarutis, V.; Pimpe, J.; Vengelis, J. Partially coherent UV–VIS light generation in photonic crystal fiber using femtosecond pulses. *Results Phys.* **2021**, *31*, 104965. [[CrossRef](#)]
20. Paul, B.K.; Moctader, M.G.; Ahmed, K.; Khalek, M.A. Nanoscale GaP strips based photonic crystal fiber with high non-linearity and high numerical aperture for laser applications. *Results Phys.* **2018**, *10*, 374–378. [[CrossRef](#)]
21. Wu, D.; Guo, Z.; Wu, Z.; Shum, P. 900 nm waveband four wave mixing generation in highly nonlinear photonic crystal fiber. *J. Opt.* **2018**, *20*, 035501. [[CrossRef](#)]
22. Yuan, J.; Kang, Z.; Li, F.; Zhou, G.; Sang, X.; Wu, Q.; Yan, B.; Zhou, X.; Zhong, K.; Wang, L.; et al. Polarization-dependent intermodal four-wave mixing in a birefringent multimode photonic crystal fiber. *Opt. Lett.* **2017**, *42*, 1644–1647. [[CrossRef](#)]

23. Das, S.; De, M.; Singh, V.K. Single mode dispersion shifted photonic crystal fiber with liquid core for optofluidic applications. *Opt. Fiber Technol.* **2019**, *53*, 102012. [[CrossRef](#)]
24. Monfared, Y.E.; Liang, C.; Khosravi, R.; Kacerovska, B.; Yang, S. Selectively toluene-filled photonic crystal fiber Sagnac interferometer with high sensitivity for temperature sensing applications. *Results Phys.* **2019**, *13*, 102297. [[CrossRef](#)]
25. Wadsworth, W.; Percival, R.; Bouwmans, G.; Knight, J.; Birks, T.; Hedley, T.; Russell, P. Very High Numerical Aperture Fibers. *IEEE Photon. Technol. Lett.* **2004**, *16*, 843–845. [[CrossRef](#)]
26. Hansen, K.P.; Broeng, J.; Petersson, A.; Nielsen, M.D.; Skovgaard, P.M.W.; Jakobsen, C.; Simonsen, H.R. High-power photonic crystal fibers. *Proc. SPIE* **2006**, *6102*, 61020B. [[CrossRef](#)]
27. Olausson, C.B.; Hansen, K.P.; Broeng, J.; Noordegraaf, D.; Maack, M.D.; Alkeskjold, T.T.; Laurila, M.; Nikolajsen, T.; Skovgaard, P.M.W.; Sørensen, M.H.; et al. Airclad fiber laser technology. *Opt. Eng.* **2011**, *50*, 111609. [[CrossRef](#)]
28. Stepien, R.; Siwicki, B.; Pysz, D.; Stepniewski, G.; Kujawa, I.; Klimczak, M.; Buczynski, R. Characterization of a large core photonic crystal fiber made of lead–bismuth–gallium oxide glass for broadband infrared transmission. *Opt. Quantum Electron.* **2014**, *46*, 553–561. [[CrossRef](#)]
29. Tefelska, M.M.; Ertman, S.; Wolinski, T.R.; Mergo, P.; Dabrowski, R. Large Area Multimode Photonic Band-Gap Propagation in Photonic Liquid-Crystal Fiber. *IEEE Photon. Technol. Lett.* **2012**, *24*, 631–633. [[CrossRef](#)]
30. Amitonova, L.V.; Descloux, A.; Petschulat, J.; Frosz, M.H.; Ahmed, G.; Babic, F.; Jiang, X.; Mosk, A.P.; Russell, P.; Pinkse, P.W.H. High-resolution wavefront shaping with a photonic crystal fiber for multimode fiber imaging. *Opt. Lett.* **2016**, *41*, 497–500. [[CrossRef](#)]
31. Gloge, D. Optical Power Flow in Multimode Fibers. *Bell Syst. Tech. J.* **1972**, *51*, 1767–1783. [[CrossRef](#)]
32. Rousseau, M.; Jeunhomme, L. Numerical Solution of the Coupled-Power Equation in Step-Index Optical Fibers. *IEEE Trans. Microw. Theory Tech.* **1977**, *25*, 577–585. [[CrossRef](#)]
33. Saitoh, K.; Koshiha, M. Empirical relations for simple design of photonic crystal fibers. *Opt. Express* **2005**, *13*, 267–274. [[CrossRef](#)] [[PubMed](#)]
34. Simović, A.; Drljača, B.; Savović, S.; Djordjevich, A.; Min, R. Investigation of bandwidth in multimode graded-index plastic optical fibers. *Opt. Express* **2021**, *29*, 29587–29594. [[CrossRef](#)]
35. Tanaka, T.P.; Yamada, S. Steady-state characteristics of multimode W-type fibers. *Appl. Opt.* **1979**, *18*, 3261–3264. [[CrossRef](#)]
36. Savović, S.; Kovačević, M.S.; Simović, A.; Kuzmanović, L.; Drljača, B.; Djordjevich, A. Method for investigation of mode coupling in multimode step-index silica photonic crystal fibers. *Optik* **2021**, *246*, 167728. [[CrossRef](#)]
37. Savović, S.; Drljača, B.; Kovačević, M.S.; Djordjevich, A.; Bajić, J.S.; Stupar, D.Z.; Stepniak, G. Frequency response and bandwidth in low NA step index plastic optical fibers. *Appl. Opt.* **2014**, *53*, 6999–7003. [[CrossRef](#)]